AGU PUBLICATIONS

Water Resources Research

RESEARCH ARTICLE
10.1002/2014WR015302

Assimilation of point SWE data into a distributed snow cover model comparing two contrasting methods

Jan Magnusson[1], David Gustafsson[2,3], Fabia Hüsler[4], and Tobias Jonas[1]

[1]WSL Institute for Snow and Avalanche Research SLF, Davos Dorf, Switzerland, [2]Swedish Meteorological and Hydrological Institute, Research and Development Hydrology, Norrköping, Sweden, [3]KTH Royal Institute of Technology, Department of Sustainable Development, Environmental Science and Engineering, Stockholm, Sweden, [4]Institute of Geography and Oeschger Center for Climate Change Research, University of Bern, Bern, Switzerland

Key Points:
- Evaluating methods for assimilating snow observations into distributed models
- Assimilation can improve model skill also at locations without observations
- Assimilation of fluxes appears more successful than assimilation of states

Correspondence to:
J. Magnusson,
magnusson@slf.ch

Citation:
Magnusson, J., D. Gustafsson, F. Hüsler, and T. Jonas (2014), Assimilation of point SWE data into a distributed snow cover model comparing two contrasting methods, *Water Resour. Res.*, *50*, doi:10.1002/2014WR015302.

Received 15 JAN 2014
Accepted 6 SEP 2014
Accepted article online 11 SEP 2014

Abstract In alpine and high-latitude regions, water resource decision making often requires large-scale estimates of snow amounts and melt rates. Such estimates are available through distributed snow models which in some situations can be improved by assimilation of remote sensing observations. However, in regions with frequent cloud cover, complex topography, or large snow amounts satellite observations may feature information of limited quality. In this study, we examine whether assimilation of snow water equivalent (SWE) data from ground observations can improve model simulations in a region largely lacking reliable remote sensing observations. We combine the model output with the point data using three-dimensional sequential data assimilation methods, the ensemble Kalman filter, and statistical interpolation. The filter performance was assessed by comparing the simulation results against observed SWE and snow-covered fraction. We find that a method which assimilates fluxes (snowfall and melt rates computed from SWE) showed higher model performance than a control simulation not utilizing the filter algorithms. However, an alternative approach for updating the model results using the SWE data directly did not show a significantly higher performance than the control simulation. The results show that three-dimensional data assimilation methods can be useful for transferring information from point snow observations to the distributed snow model.

1. Introduction

In many mountainous regions, snowmelt dominates the runoff, and the timing of melt-related discharge can vary largely from year to year [*Barnett et al.*, 2005; *Stewart et al.*, 2004]. Accurately monitoring this snow storage and quantifying subsequent runoff is important for regulating lake levels and hydropower production [*Schaefli et al.*, 2007]. Additionally, melting snow can contribute to floods imposing large damages on infrastructure [*Li and Simonovic*, 2002].

A wide range of methods exist for monitoring the spatial and temporal evolution of snow water resources. The most commonly used techniques for spatially estimating snow amounts include interpolation schemes [*Harshburger et al.*, 2010; *Lopez-Moreno and Nogues-Bravo*, 2006], remote sensing [*Pulliainen*, 2006], parametric snow cover models [*Ohmura*, 2001; *Tobin et al.*, 2013], and models based on physical principles [*Essery et al.*, 2013; *Marks and Winstral*, 2001]. Driven by weather forecasts, the two types of models can be used for prognostic snowmelt simulations required for flood forecasting. For accurate predictions, the models require correct initial conditions such as snow water equivalent (SWE) and snowpack wetness, as well as correct meteorological forcing during the forecast period. During the course of a season, errors in estimates of snowfall and snowmelt accumulate and can result in inaccurately modeled snow conditions at the start of a forecast period. The errors arise primarily due to uncertain input data and model deficiencies. Along with attempting to remove such errors and deficiencies, we currently consider that conditioning the snow simulations on observations shows a large potential for obtaining more reliable model initial conditions. Particularly for operational proposes, we see a need for improving snow cover simulations using data assimilation methods. Another common objective for using data assimilation is to quantify forecast uncertainties.

The most straightforward data assimilation method is called direct insertion, in which the modeled states, for example, SWE, are replaced with the observations at the same location [*Fletcher et al.*, 2012; *Liston et al.*, 1999]. However, this method ignores both model and observation uncertainties which is not a realistic

simplification in the case of snow simulations. In addition, all locations lacking observations typically remain uninfluenced by this basic data assimilation scheme. For distributed models, one method is to adapt the parameters influencing snow accumulation and snowmelt by creating correction factors derived from interpolated fields of model residuals as presented in *Liston and Hiemstra* [2008], who also discuss the possibility to include model and observation uncertainties in this method. Another approach for including uncertainties into the analysis is optimal interpolation (sometimes called statistical interpolation), in which the relative weight between the model and observation uncertainties influence the amount of correction performed by the data assimilation routine. This method has been shown to improve the accuracy of snow depth estimates at continental scales [*Barnett et al*., 2005; *Brown et al*., 2003] as well as snow distributions obtained by remote sensing [*Liu et al*., 2013]. However, in statistical interpolation, uncertainties are specified a priori and internal model states related to the updated variable remain unchanged (unless using an application-specific multivariate statistical interpolation). These drawbacks can be avoided by using generic data assimilation methods with evolving error statistics. Examples of such methods which have been used for snow simulations include the ensemble Kalman filter [*Andreadis and Lettenmaier*, 2006; *De Lannoy et al*., 2012; *Slater and Clark*, 2006] and the particle filter [*Leisenring and Moradkhani*, 2011]. However, most of these prior studies for snow do not use three-dimensional data assimilation methods. Such schemes make use of spatially correlated error statistics to influence unobserved locations required for distributed model applications [*Reichle and Koster*, 2003].

In this study, we evaluate different methods for assimilating point snow observations in a distributed model. Our first specific aim is to evaluate whether advanced three-dimensional data assimilation methods can reliably propagate information from observation sites and improve the simulation results at locations lacking observational data for assimilation. Our second aim is to compare the model behavior and performance when assimilating states (SWE) versus assimilating fluxes (snowfall rates and melt rates). The uncertainty in the accumulated states arises from the uncertainty in the decrements/increments of the snow states (snow accumulation and melt). For this reason, updating the increments in the snow states (i.e., snow accumulation and melt) was suggested as a potential research topic for improving snow data assimilation methods [*Liu et al*., 2013]. In this study, we focus on ground observations since those typically provide the most reliable information on available snow water resources and should not be neglected in operational modeling schemes. Remote sensed observations of snow cover fraction do not provide a direct measure of snow amounts, and can additionally be missing for long periods in areas with persisting cloud cover. Furthermore, in mountain areas with large snow amounts, satellite observations cannot depict snow water equivalents reliably [*De Lannoy et al*., 2012].

2. Model and Assimilation Framework

We begin by presenting a general and site-independent description of our approach for including point snow observations into large-scale hydrological simulations (section 2), followed by a case study including a presentation of site-specific details (section 3).

2.1. Model Framework

The typical hydrological application in snow-dominated regions requires large-scale estimates of snow amounts and melt rates. To improve such estimates, we would like to include all relevant observations in the modeling procedure. In many situations, the most abundant snow measurements are ground point observations, e.g., snow depth and SWE at a given set of station locations. However, comparing point data with simulations on a course resolution grid entails problems if elevations of collocated grid cells and stations differ significantly. These problems can be mitigated if we use a snow model which represents the snow cover development both over a regular grid (for the hydrological application) and single points (for comparing against ground observations) at the same time. To accurately compute the snow cover mass balance for the gridded simulations, the model should include a depletion curve tracking the fractional snow-covered area used for scaling the simulated melt rates. In this study, we focus on the performance of the data assimilation methods. We thus use a parsimonious and computationally efficient temperature-index snow model with SWE and liquid water content as main state variables. However, note that the data assimilation procedure described below is largely independent of model type. Thus, if advantageous, the temperature-index simulations can be replaced by a more complex model (e.g., energy balance model).

2.2. Data Assimilation Methods

In this study, we apply statistical interpolation and/or ensemble Kalman filter (EnKF), which are two closely related data assimilation algorithms. Both algorithms allow for improvements of gridded simulation results using the residuals between observations and simulations obtained at point snow measurement sites. We have chosen the two methods since they are computationally efficient and do not require, for example, linearization of the model or any adjoint models. See *Clark et al*. [2008] for an overview of data assimilation methods relevant for hydrological applications. Below, we describe the data assimilation methods in general, followed by a description of how these methods can be applied for assimilating point snow observations.

2.2.1. Statistical Interpolation

Statistical interpolation (also called optimal interpolation) is a computationally efficient method to update a background field using observations. The update equation describes the correction of the model forecast using available observations for time step t_i (we follow the notation of *de Rosnay et al*. [2012], *Leisenring and Moradkhani* [2011], and *Uboldi et al*. [2008]):

$$x^a(t_i) = x^b(t_i) + K(y(t_i) - yp(t_i)) \tag{1}$$

where the vector x^a is the analysis field (updated model states), x^b is the background field (first guess of model states), K is the gain matrix, y is the observations, and yp is the so-called predicted observations (model estimates of the measurements). The gain matrix is computed using covariance matrices:

$$K = C_{xy}(C_{yy} + R)^{-1} \tag{2}$$

which are given by:

$$C_{xy} = \langle (x^b - x^t)(yp - y^t)^T \rangle \tag{3}$$

$$C_{yy} = \langle (yp - y^t)(yp - y^t)^T \rangle \tag{4}$$

$$R = \langle (y - y^t)(y - y^t)^T \rangle \tag{5}$$

where x^t is the true state, y^t is the true observation, and the angular brackets denote an average over many realizations. Thus, the gain matrix is computed using the covariance matrix between the errors of states and predicted measurements C_{xy}, the covariance matrix between the errors of predicted measurements themselves C_{yy} and the covariance matrix of observation errors R. In statistical interpolation, these error covariance matrices are defined a priori with spatial dependencies specified using analytical correlation functions.

2.2.2. Ensemble Kalman Filter

The EnKF is a sequential data assimilation algorithm with evolving error statistics represented by a finite number of ensemble members. Instead of specifying the error covariance matrices a priori as in statistical interpolation, those matrices are computed from an ensemble which is propagated forward in time using the dynamical model. This filter is only optimal with an infinite number of ensemble members, a linear dynamical model, and normally distributed errors. However, those requirements are more or less always violated but accepted in applications resulting in suboptimal filter performance. In this study, we use the standard formulation of the EnKF which we present briefly below (for a detailed description of the method see *Evensen* [2009] and references therein).

For each time step and individual location, an ensemble of model states is first propagated through the dynamic model:

$$x_j^b(t_i) = f\left(x_j^a(t_{i-1}), u_j(t_i), \theta\right) + \omega_j(t_i) \tag{6}$$

where $f(\cdot)$ is the dynamical model (in our case the snow model), u_j is the model inputs, θ represents the model parameters, ω_j is a random model error, and j is the ensemble member.

Afterward the state variables are transformed to the observation space:

$$yp_j(t_i) = h\left(x_j^b(t_i)\right) + v_j(t_i) \tag{7}$$

where yp_j is the predicted observation and v_j is the observation error.

In contrast to statistical interpolation, where the error covariance matrices are defined a priori, the ensemble spread around its mean (as substitute for the true values) is used for computing those matrices (compare with equations (3)–(5)). The model ensembles for different locations need to be correlated so that information from the observation sites can influence locations lacking measurements [*Reichle and Koster*, 2003]. Such correlations are typically produced by perturbing the input data assuming spatially correlated errors. In this study, we perturb the desired input variables using random correlated fields generated with a fast Fourier transform algorithm. The random fields are generated on a regular two-dimensional grid and afterward interpolated to the model grid and the point observation sites.

The topography influences accumulation and melt of snow strongly. Often observations on differing altitudes show very different behavior. We therefore apply covariance localization to suppress unrealistic covariances arising between sites located close to each other horizontally but on different altitudes. Such covariances can arise from the purely two-dimensional random number generator which was selected for computational efficiency. Additionally, the method also suppresses unrealistic covariances arising from the limited number of ensemble members. Covariance localization was included by modifying the gain matrix following *Oke et al*. [2007]:

$$K = \rho_{xy} \circ C_{xy}(\rho_{yy} \circ C_{yy} + R)^{-1} \tag{8}$$

where the scalar matrices ρ_{xy} and ρ_{yy} restrict the influence of the observations on the updated variables using the element-wise product (also called Hadamard and Schur product). Those scalar matrices are defined by distance-dependent functions converging toward zero at appropriate separation lengths.

2.3. Strategies for Snow Data Assimilation

In this section, we assume that we have SWE observations available, and that we have a model with SWE as its main state variable. We present two approaches below for assimilating daily point observations of SWE. There are, of course, many more strategies for including such measurements into the modeling procedure. See the site-specific application of our methods for details about the filter setup (section 3.4).

2.3.1. Assimilating States

Perhaps, the most obvious approach for updating the model state variables (SWE and liquid water content in our case) is to directly assimilate observed snow water equivalents. In this approach, we generate ensemble members, for both the point observation sites and the model grid, using interpolated input data perturbed with spatially correlated errors. For each time step, we update the simulated SWE and liquid water content for both the point observation sites and the model grid. For this task, we use the EnKF since this assimilation method allows us to update internal state variables, liquid water content for our model, indirectly using the SWE observations.

2.3.2. Assimilating Fluxes

In this approach, we split the data assimilation problem into smaller pieces, which can be of advantage compared to solving a larger problem directly [*Liu et al*., 2012]. We update the simulation results by assimilating fluxes (snowfall and melt rates) instead of states (snow water equivalents). In a first step, we simulate snow accumulation and update the results using snowfall rates inferred from daily observations of SWE. Thus, in this step, we update the precipitation forcing provided to the snow model. For this task, we use statistical interpolation because (a) we do not need to update any internal state variables which have not been observed, and (b) the solution given by statistical interpolation is exact in contrast to methods relying on a finite number of ensemble members. In a second step, we compute snowmelt rates using the temperature-index method. We update the simulated melt rates and the two model state variables (SWE and liquid water content) with the EnKF using melt rates computed from daily SWE observations.

3. Site-Specific Application

We first present the data available for our particular study site, followed by a description of our snow model including parameter identification. We then explain how we apply the general methods presented above in two site-specific data assimilation experiments. We also report about a benchmark method for estimating snow water equivalents at unobserved locations.

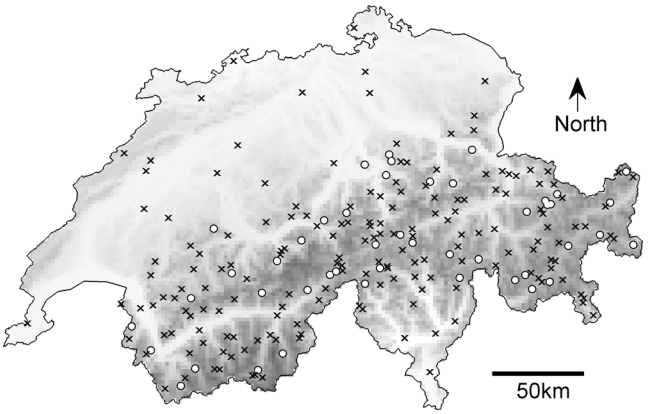

Figure 1. Study area with snow depth measurement locations (crosses) and in situ snow water equivalent observation sites (circles) used in this study.

3.1. Study Site and Data

3.1.1. Data Used for Calibration and Assimilation

Our study area, Switzerland, covers an area of 41,285 km^2 and an altitude range from 193 to 4634 m (Figure 1). For our data assimilation experiments, we use snow water equivalents estimated from daily point measurements of snow depth from both automatic measurement stations and manual observations. The measurements are made in flat open terrain and cover an altitude range from 230 to 2950 m. Both the automatic and manual snow depth measurements were recorded at around 08:00 h. The snow data set has previously been used for operational monitoring of snow water resources. For this purpose, the measurements were visually checked for missing or faulty data. Data gaps and erroneous data were replaced by appropriate gap filling methods, considering measurements recorded at the same station at previous and subsequent time steps as well as observations from neighboring stations.

In our general description of the data assimilation methods (see section 2.3), we assumed that daily SWE observations were available. At our study site, however, we possess more snow depth than SWE observations. Due to this, we convert daily point measurements of snow depth to water equivalent (Figure 2, top plots) using a snow density model before assimilation. The model deployed here is based on methods presented by *Martinec and Rango* [1991] and describes accumulation and densification of the snowpack layer by layer. The original density model has been modified and recalibrated based on data from over 10,000 snow profiles presented in *Jonas et al*. [2009]. These modeled snow water equivalents were used both for model calibration and within the data assimilation experiments. From the increments/decrements in snow water equivalent, we also compute snowfall and melt rates (Figure 2, bottom plots). We thus assume that

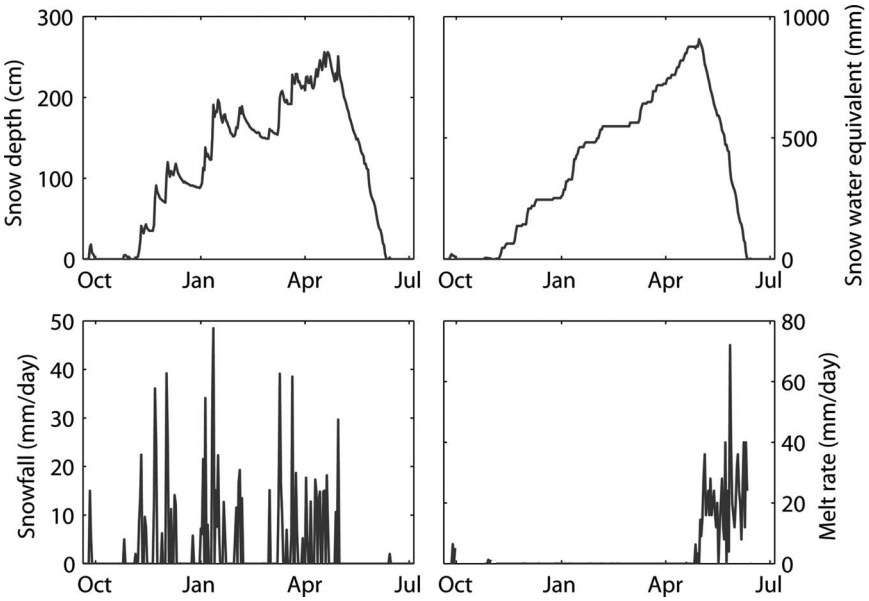

Figure 2. (top right) Example of snow water equivalent computed from (top left) snow depth measurements at an arbitrary station for one winter. From the computed snow water equivalent, we can estimate (bottom left) snowfall rates and (bottom right) melt rates for each day.

accumulation and melting do not occur at the same time. This assumption may result in small errors, but typically melt rates are small during snowfall episodes.

3.1.2. Snow Water Equivalent Data Used for Model Evaluation

We used snow water equivalents measured manually (stations represented by circles in Figure 1) for the model evaluation (see results in section 4). These measurements are made every second week at 45 locations throughout the Swiss Alps. The observation sites cover an altitude range from 1195 to 2697 m. The water equivalents are measured by extracting snow cores using an aluminum tube with a cross-sectional area of 70 cm^2. In the data assimilation experiments described below, we removed all other snow observations closer than 3 km to the sites with SWE measurements so that the evaluation points mimic locations lacking data for assimilation.

In the following, we denote the different snow water equivalents used in this study as follows:

1. SWE_{OBS}—observed snow water equivalents used for evaluating the data assimilation experiments.
2. SWE_{HS}—snow water equivalents computed from the snow depth recordings.
3. SWE_{SIM}—snow water equivalents simulated by the temperature-index model described below (section 3.2).

3.1.3. Satellite Observations Used for Model Evaluation

Daily snow-covered area at approximately 1 km spatial resolution is derived from the AVHRR sensor on the NOAA-platform and MetOp-platform. The automated snow detection capitalizes on the distinct optical properties of snow with high reflectance in the visible wavelengths and low reflectance in the near-infrared part of the electromagnetic spectrum. The retrieval algorithm was originally developed for rather flat areas in Canada [*Khlopenkov and Trishchenko*, 2007] and has been adapted and optimized for use in complex terrain [*Huesler et al*., 2012]. The modifications of the original algorithm include changes in the thresholds, taking into account the land cover types and topographic features such as orographic shadows. The output of the snow processing consists of binary snow maps for Switzerland, which we use for validation of the snow model simulations.

The automated detection algorithm mapped snow with an accuracy of approximately 90% (probability of detection) depending on landcover, season, and topographic complexity [*Huesler et al*., 2012]. For the majority of optical satellite snow products, most uncertainties arise from incorrect cloud-snow discrimination as well as from forest-covered areas where snow on the ground is masked by canopy. To avoid uncertainties arising from obstacles masking the ground, we excluded nodes of the satellite grid containing much forest and buildings (>30% coverage). For these landcover types, neither the satellite images nor our snow model provide reliable information about snow coverage.

3.1.4. Model Input Data

The model applied in this study requires two inputs: daily average air temperature and daily total precipitation. Air temperatures at simulation points were obtained using data from 228 stations covering altitudes between 197 and 3580 m following methods similar to *Frei* [2013]. In mountainous regions, temperature lapse rates are often nonlinear due to, for instance, inversion layers. Therefore, we first removed the vertical temperature trend by fitting a parametric nonlinear curve to the data assuming a spatially stationary profile. Afterward, we used an inverse distance weighting scheme to interpolate the residual temperatures to the simulation points (grid and stations). We used the following distance measure d (m) in the interpolation scheme [see also *Foppa et al*., 2007]:

$$d = \sqrt{d_h^2 + p d_v^2} \tag{9}$$

where d_h (m) describes the horizontal separation distance between a station and a simulation point and d_v (m) describes the vertical separation length. For each day, the weighting factor p (dimensionless) was estimated by minimizing the error in a leave-one-out cross-validation procedure. A large value on this weighting factor reduces the influence of stations horizontally close to a simulation point but on a differing altitude. Finally, the nonlinear temperature lapse rate was added to the interpolated residual values. See *Frei* [2013] for a detailed assessment of the method, we adopted for this study.

We use the gridded precipitation product RhiresD provided by MeteoSwiss for model input which provide daily total precipitation estimates with a spatial resolution of approximately 2 by 2 km. The spatial analysis for RhiresD was accomplished using approximately 440 rain gauge measurements across Switzerland, adopting an angular distance weighting scheme [*Frei and Schar*, 1998; *Shepard*, 1984] in combination with a

high-resolution long-term climatology [*Schwarb et al*., 2001], see also section 4.1 of *Frei et al*. [2006]. Error statistics and characteristics of the resulting fields are like those described in *Isotta et al*. [2013]. For mountainous regions, a leave-one-out cross-validation shows typical relative errors of about 25% for moderate intensity rainfall. Higher intensity precipitation events display somewhat lower uncertainty, whereas precipitation events with lower intensity show higher uncertainty. Note that the precipitation product was generated using stations mainly on lower elevations (below 1200 m) and, hence, the measures of uncertainty at high elevations are likely even larger than these numbers. The interpolation was accomplished without including corrections for gauge undercatch. Therefore, the interpolation systematically underestimates precipitation during periods with snowfall. We interpolated the gridded precipitation estimates to the simulation points using a nearest neighbor approach if necessary.

In conclusion, all input and assimilation data sets feature considerable shortcomings but represent a typical constraint for operational model applications such as snow water resources monitoring.

3.2. Snow Model

3.2.1. Computing Snow Accumulation

Typically, snow models contain several step functions, such as the separation of precipitation into liquid and solid phases. Using these kinds of functions in models may lead to noisy response surfaces during calibration [*Kavetski and Kuczera*, 2007] as well as likely causing undesired jumps between ensemble members used in some data assimilation schemes. To minimize such numerical problems, we use smoothed functions instead of step functions in our model [see *Kavetski and Kuczera*, 2007, for details].

The amount of snowfall, P_s (mm/d), is given by daily total precipitation, P_{tot} (mm/d), daily average air temperature, T (°C), a precipitation correction factor accounting for gauge undercatch, P_{corr} (dimensionless), and a threshold temperature, T_{pbase} (°C), below which precipitation falls mainly as snow:

$$P_s = P_{tot}\frac{P_{corr}}{1+\exp(T_p)} \tag{10}$$

where $T_p = (T - T_{pbase})/m_p$. The parameter m_p (°C) determines the temperature range for mixed precipitation.

3.2.2. Computing Snowmelt

We use the temperature-index method to compute the daily amount of snowmelt, M (mm/d), occurring above a certain threshold temperature, T_{mbase} (°C):

$$M = MF\ m_m(T_m + \ln(1+\exp(-T_m))) \tag{11}$$

where MF (mm °C^{-1} d^{-1}) is the melt factor and $T_m = (T - T_{mbase})/m_m$. Here the parameter m_m (°C) determines the smoothness of the transition where snow begins to melt depending on temperature. Melt cannot exceed the amount of ice in the snowpack. To reduce the number of calibration parameters, we assume that T_{mbase} equals 0°C and that m_m equals 0.5°C. The melt factor typically shows seasonal variations, and including such effects in the model usually improves the snow cover simulation quality considerably [*Rango and Martinec*, 1995]. To take seasonal variations of the melt factor into account, we follow the approach described by *Slater and Clark* [2006]:

$$MF = \frac{MF_{min} + MF_{max}}{2} + \frac{MF_{max} - MF_{min}}{2}\sin\left(\frac{2\pi n}{365}\right) \tag{12}$$

where MF_{min} is the minimum melt factor occurring at winter solstice, MF_{max} is the highest melt factor occurring at summer solstice, and n is the day-number starting at the 21 March.

We also allow the snow cover to hold liquid water by introducing a second state variable, the liquid water content which we define as the mass ratio of liquid water to snow water equivalent stored in the snowpack. Melt and rain water first leaves the snow when the fraction of liquid water exceeds the so-called maximum water holding capacity which is a tuneable parameter.

3.2.3. Computing Snow-Covered Fraction

The model equations described above depict the snow cover development at single points, such as measurement stations. For computing the snow storage evolution over an area (such as a model grid cell), we need to estimate the fractional snow-covered area along with the accumulation and ablation rates. The

accumulation rates given by precipitation apply to the whole area, whereas the ablation rates given by the temperature-index method only apply to the snow-covered part of the same area.

We compute snow-covered fraction, *SCF* (dimensionless), from simulations of the grid cell average snow water equivalent, $\overline{SWE}_{SIM}$ (mm), using the parameterization presented by *Essery and Pomeroy* [2004]:

$$SCF = \tanh\left(1.26 \frac{\overline{SWE}_{SIM}}{CV\overline{SWE}_{MAX}}\right) \quad (13)$$

where *CV* (dimensionless) denotes the coefficient of variation and $\overline{SWE}_{MAX}$ (mm) is the highest average SWE occurring before the onset of melt. This parameterization is derived assuming that the snow cover prior to melt follows a lognormal probability distribution and that melt occurs uniformly. The parameterization was validated against depletion curves derived theoretically for coefficient of variations between 0.1 and 0.5. The equation only describes the snow-covered area development correctly in the case of a continuous accumulation phase followed by an ablation period uninterrupted by snowfalls. We address this problem heuristically by adding a second snow storage in the case of snowfall after melting has started. For a snowpack going through several cycles of accumulation and melting, algorithms such as ours may fail to capture the snow-covered area accurately.

3.3. Identification of Model Parameters

The parameters needed for computing the precipitation phase were determined using observed daily average air temperatures, precipitation sums, and new snow depths. We used data available from 29 stations located throughout Switzerland, spanning an altitude range from 316 to 2690 m and covering the period 1 January 2000 to 31 December 2012. At these locations, precipitation was measured with heated gauges (0.1 mm resolution) and new snow depths were observed manually (1 cm resolution). We rounded the precipitation observations to integer values before analysis to have a consistent resolution between the two types of measurements. Afterward, we approximated the relation between precipitation phase and air temperature by computing the relative frequency of snowfall occurrences to observed precipitation events for temperature categories of 0.5°C (Figure 3). Finally, we fitted the two parameters influencing the precipitation phase ($T_{pbase} = 1.0$°C, $m_p = 1.24$) by minimizing the squared errors between the modeled and observed fraction of snowfall events.

The precipitation correction factor was estimated using snowfall amounts inferred from the snow depth observations (see section 3.1.1 and Figure 2). We used stations where both snow depths and air temperatures have been recorded at the same time. For the calibration, we chose a period (15 October 2002 to 1 August 2006) nonoverlapping with the data assimilation experiments presented below. At these stations, we modeled snowfall amounts using the precipitation model (equation (10)) with the recorded air temperatures and total precipitation amounts (interpolated using RhiresD data, see section 3.1.4) as input. The snowfall amounts computed from the snow depth recordings were approximately 20% higher than the simulation results.

The remaining parameters of the model were calibrated largely following the methods presented by *Kokkonen et al*. [2006]. We first generated parameter combinations on regular intervals in the range of a feasible parameter space. For each parameter combination, we judged the model performance by (a) computing the normalized root-mean-squared-error between the SWE_{SIM} and SWE_{HS} for each station and (b) afterward computing the average of those errors. For the model calibration, we used the same calibration period and set of stations as for identifying the precipitation correction factor. As precipitation input at each station, we used snowfall amounts inferred from the snow depth observations (SWE_{HS}). With this approach, we ensure that the precipitation input data to the model is consistent with the validation data set. Then the calibration routine should produce parameter values which reflect the processes of melting and liquid water holding capacity of the snowpack. If, for example, we would have used inaccurate precipitation input, the optimized parameters may have deviated from the desired outcome due to compensating mechanisms caused by biased input.

The calibration results showed that the parameters could be identified within a defined range (Figure 4). These well-defined parameters are due to a parsimonious model structure with few tuneable parameters. Including more processes, such as refreezing of liquid water in the snowpack, introduced more parameters to the model but did not improve the simulation quality. The additional parameters could also not be

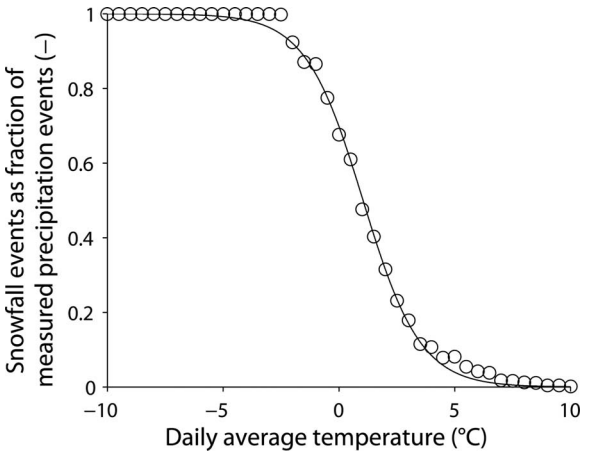

Figure 3. Fraction of snowfall events as function of daily average air temperature. The circles display the observations and the curve shows the fitted parametric curve.

constrained by the available data. The optimal parameter value for the minimum melt factor equal 0.5 mm $^{\circ}C^{-1}$ d^{-1}, the maximum melt factor equal 3.9 mm $^{\circ}C^{-1}$ d^{-1} and, the maximum water holding capacity equal 0.04 (dimensionless). The optimal simulation results show a high correlation equal 0.98 and low normalized root-mean-squared-error equal 9% with the reference SWE records. Since the precipitation to the model was derived from the validation data, the above presented model performance should be judged critically. Nevertheless, the high model performance indicates that simulations follow the validation data closely during the snowmelt season which was the aim of our calibration. The advantage of using the reference snow water equivalents (SWE_{HS}) for parameter calibration is the large data availability. Obviously, the disadvantage is that those data are not as trustworthy as direct observations of snow water equivalent. However, the SWE observations are less frequently available and providing accurate snowfall estimates at those sites necessary for reliable calibration would have introduced an additional source of uncertainty.

We assume a subgrid premelt coefficient of variation for SWE equal to 0.5 when computing snow-covered fraction. This value is within the range reported for midlatitude prairie landscapes [*Clark et al*., 2011] and should be representative for most nonforest areas below 1500 m at our study site. The snow cover in mountainous regions show higher premelt variability than for flatter landscapes, and for a high elevation site in our study domain coefficient of variation values around 0.8 have been reported [*Egli et al*., 2012]. However, those areas only cover around 20% of Switzerland, and the parameterization by *Essery and Pomeroy* [2004] does not support such high coefficient of variations.

3.4. Description of Data Assimilation Experiments

In the following, we describe two site-specific numerical experiments using the data assimilation methods proposed above (see section 2). The results of these two experiments are compared against a control simulation without using data assimilation and a benchmark method for interpolating snow water equivalents.

For our data assimilation experiments, we simulate the snowpack development from 1 August 2006 to 1 August 2009 for four different types of locations:

1. The stations with daily SWE data computed from snow depth observations (see section 3.1.1) at which we can update the simulated snow water equivalents (see crosses in Figure 1). We thus study how information from these stations spread to the three remaining types of locations in our data assimilation experiments described below.

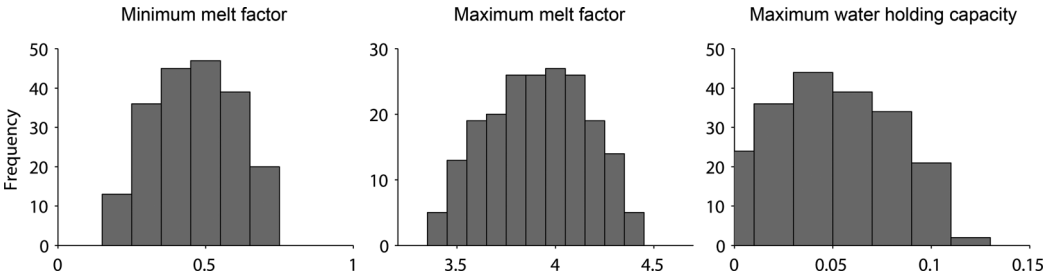

Figure 4. Marginal distributions of calibrated parameter values for the snow model.

2. The nodes of a regular grid used in distributed model simulations (2 km resolution). We use these simulations for visualizing how the data assimilation scheme influences spatial estimates of, for example, snow water equivalents and melt rates.
3. The field sites with in situ SWE observations available every second week during winter (see circles in Figure 1). At these locations, we can evaluate the performance of the model and data assimilation scheme using independent measurements.
4. The nodes of the satellite images providing binary information about snow coverage. This data covering large areas provide an additional source of information for model validation.

3.4.1. Experiment 1—Assimilating States

We apply the EnKF to update the model states using snow water equivalents computed from snow depth records (see also section 2.3). We use 100 ensemble members in all simulations presented in this study. Appropriately estimating the error statistics for the input and observation data is not trivial in data assimilation studies as discussed by *Slater and Clark* [2006]. For this reason, error statistics are often defined using simple and subjective approaches [*Andreadis and Lettenmaier*, 2006; *Clark et al*., 2008; *Weerts and El Serafy*, 2006] or sometimes adjusted to optimize filter performance [*Reichle and Koster*, 2003]. In this study, we define the necessary uncertainty measures based on earlier studies, see references below, with adjustments to achieve satisfactory filter performance. For air temperature, we adopted the spatial error correlation structure suggested by *Uboldi et al*. [2008]:

$$r = \exp\left(-\frac{d_h^2}{L_h^2}\right) \tag{14}$$

where r (dimensionless) is the correlation between two points, d_h (m) is the horizontal distance between points, and L_h (m) is the horizontal correlation length scale. We perturb the interpolated air temperatures using normally distributed noise with a horizontal correlation length of 60 km and a standard deviation of 2°C. For total precipitation, we specify a slightly different exponential correlation function based on initial investigation of the model error in snow accumulation and following *Clark et al*. [2008]:

$$r = \exp\left(-\frac{d_h}{L_h}\right) \tag{15}$$

with a correlation length L_h of 30 km. We generate the precipitation ensemble by adding a normally distributed perturbation with standard deviation σ_P (mm/d) as a fraction of total precipitation:

$$\sigma_P = 0.5 * P_{tot} \tag{16}$$

The uncertainty of the precipitation fields given above (see section 3.1.4) did not take the additional uncertainties associated with measuring snowfall compared to rainfall into account. For this reason, we assume higher errors in the precipitation estimates than presented by *Isotta et al*. [2013].

We apply a localization function to suppress any unrealistic covariances arising from the limited number of ensemble members, and the purely two-dimensional random number generator which was selected for computational efficiency (see section 2.2.2). A localization function of the following form was applied:

$$\rho = \exp\left(-\frac{d_h^2}{L_h^2}\right)\exp\left(-\frac{d_v^2}{L_v^2}\right) \tag{17}$$

where in this equation the horizontal L_h and vertical L_v separation distances determines the influence radius of the observations, which should not be confused with the correlation length scales given in equations (14), (15), and (19). We set L_h equal to 80 km and L_v equal to 500 m. Note that the horizontal length scale used in the localization function exceeds those applied in equations (14) and (15).

We assume spatially uncorrelated observation errors with standard deviation $\sigma_{SWE_{HS}}$ (mm) as a fraction of the snow water equivalents computed from the snow depth records including a constant error term:

$$\sigma_{SWE_{HS}} = 0.3 * SWE_{HS} + 5 \tag{18}$$

3.4.2. Experiment 2—Assimilating Fluxes

In this experiment, we update the simulation results by assimilating fluxes (snowfall and melt rates) instead of states (snow water equivalents). For each time step, we first use statistical interpolation to improve the simulated snowfall rates. We generate a background field of P_s using equation (10) which we update using snowfall rates P_{HS} inferred from the snow depth records (see section 3.1.1). For the assimilation, we update the background field using equations (1) and (2). Afterward, we propagate the ensemble of state variables through the snow model (equation (6)) with perturb air temperature and replicates of the updated snowfall field as input. This step provides us with background fields of SWE, liquid water content, and melt rate for the different types of locations available (see description above). We use the melt rates computed from the snow depth records (see section 3.1.1) to update those three fields using equations (1) and (8). The specification of the error statistics follows below.

In statistical interpolation, we can define three-dimensional correlation structures without any loss in computational efficiency as opposed to ENKF method (see description above). We can directly include the vertical dimension in the correlation function and do not have to suppress vertical correlations by using a localization function. Thus, in the first data assimilation step, we assume the following spatial correlation structure for errors of the snowfall background fields:

$$r = \exp\left(-\frac{d_h}{L_h}\right)\exp\left(-\frac{d_v^2}{L_v^2}\right) \tag{19}$$

which is a combination of the horizontal component used in equation (15) and the vertical component applied in equation (17). We use the same parameters as in experiment 1 (see above), a horizontal correlation length scale L_h equal to 30 km and a vertical correlation length scale L_v equal to 500 m.

The errors of simulated snowfall can be large because (a) the total precipitation fields are uncertain, particularly at the point scale, (b) the snowfall correction factor can be time dependent, (c) most stations used for generating the total precipitation fields were located on elevations below 1200 m and, (d) the simulated snowfall rates are sometimes affected by misclassification of precipitation type. We specify the errors of the background field as a standard deviation σ_{P_s} (mm/d) given by the fraction of total precipitation including a constant error term times a scaling factor sf (dimensionless):

$$\sigma_{P_s} = sf(0.5 * P_{tot} + 5) \tag{20}$$

The scaling factor reduces the errors for air temperatures at which snowfalls are unlikely:

$$sf = \frac{1}{1+\exp(T_p)} \tag{21}$$

where $T_p = (T - T_{pbase})/m_p$. For this equation, we choose T_{pbase} equal 7.5°C and m_p equal 1 (dimensionless). Note that with statistical interpolation, we can assign a constant error term without any complications opposed to the ensemble-based methods which do not allow unrealistic states, such as negative precipitation rates (compare equations (16) and (20)).

The snowfall rates P_{HS} (mm/d) inferred from the snow depth measurements are uncertain foremost because (a) the areal representation of the station recordings are unknown, (b) of errors in the snow depth measurements, and (c) due to errors in the model converting snow depth recordings into snow water equivalents. Here we define the standard deviation of the observation errors $\sigma_{P_{HS}}$ (mm/d) as a fraction of the estimated snowfall amounts including a constant error term:

$$\sigma_{P_{HS}} = 0.3 * P_{HS} + 3 \tag{22}$$

We further assume that the observations errors are spatially uncorrelated.

In the second data assimilation step, we update the model state variables with the melt rates inferred from the snow depth observations using the EnKF. Therefore, we only consider the uncertainty in the air temperature input data since the snowfall input does not influence the ablation rates. We assume a spatial correlation structure for air temperature following equation (14) with the horizontal correlation length scale equal 60 km. We again perturb the interpolated air temperatures using normally distributed noise with a standard deviation equal to 2°C.

We also assume that the observation errors, in this case the melt rates inferred from the snow depth observations M_{HS}, are spatially uncorrelated. We specify the standard deviation of observation error (mm/d) as a fraction of the computed melt rates including a constant error term:

$$\sigma_{M_{HS}} = 0.1 * M_{HS} + 1 \tag{23}$$

3.5. Benchmark Method for Predicting Snow Water Equivalents

We compare the results from the data assimilation experiments against an independent method for estimating snow water equivalent at unobserved locations. With this test, we can investigate whether the data assimilation methods which combines three variables (air temperature, total precipitation, and snow water equivalent) improves the SWE estimates compared to a method relying on only one of these data sources.

For each day, we spatially interpolate the snow water equivalent to the validation points following the methods of *Foppa et al*. [2007]. First, we compute a base value describing the relationship between snow water equivalent with elevation using a power function. Afterward, we compensate for regional deviations from the base value using a compensation value:

$$\mathrm{SWE}_{\mathrm{INT}}^{\mathrm{k}} = \mathrm{G}\left(\mathrm{z}^{\mathrm{k}}\right) + \mathrm{A}^{\mathrm{k}} \tag{24}$$

where $\mathrm{SWE}_{\mathrm{INT}}^{\mathrm{k}}$ is interpolated snow water equivalent (mm) at the target station, $\mathrm{G}\left(\mathrm{z}^{\mathrm{k}}\right)$ is the base value (mm), z^{k} is the elevation (m), A^{k} is the regional compensation value (mm), and k is the index of the target station. The compensation value is computed using three stations in the neighborhood of the target station:

$$\mathrm{A}^{\mathrm{k}} = \sum_{\mathrm{i}=1}^{3} \frac{\mathrm{SWE}_{\mathrm{HS}}^{\mathrm{i}} - \mathrm{G}^{\mathrm{i}}}{3} \tag{25}$$

The three neighboring stations were selected based on the distance measure presented in equation (9) with $p = 5000$. See *Foppa et al*. [2007] for a detailed description of this interpolation method developed and optimized for Switzerland.

4. Results and Discussion

4.1. Differences in Behavior Between the Assimilation Methods

Figure 5 illustrates the behavior of both assimilation methods in scenarios where SWE is underestimated or overestimated compared to the data available for assimilation. The first example shows that during accumulation both assimilation methods increase the snowfall amounts (see blue and green lines in Figure 5a) which were underestimated by the control simulation compared to the assimilation data (see red solid and black dashed lines in Figure 5a). The flux assimilation method follows a stepwise increase in SWE whereas the state assimilation method displays a gradual increase even during periods lacking snowfall in the other time series. The second example shows that during ablation the flux assimilation method approximately follows the decline rate in SWE of both the control simulation and $\mathrm{SWE}_{\mathrm{HS}}$ time series (Figure 5b). The state assimilation method, on the other hand, forces simulated SWE during ablation toward the assimilation data inducing higher melt rates than in any of the other time series. The third example illustrates a location where the state assimilation strongly forces the simulation toward the data used for updating the model (Figure 5c). The flux assimilation approach rather follows the control simulation and several of the neighboring stations. The three examples presented above indicate that for accurate observations of variables showing low representativeness errors the state assimilation method seems appropriate since the updated simulation appears to follow the assimilation data closely. However, for observations showing large spatial variations and strong autocorrelations in time (such as point snow measurements), the state assimilation method may follow the assimilation data too strongly, and the flux assimilation seems to be a more appropriate choice. Additionally, snowmelt rates directly influence the stream discharge. Thus, in hydrological modeling, improving simulated melt fluxes rather than the snow states by data assimilation can be more effective for improving streamflow simulations.

4.2. Snowfall Estimates

The control simulation, without data assimilated, provides snowfall estimates which sometimes differ largely from the snowfall inferred from the snow depth observations (Figure 6, left). In the depicted

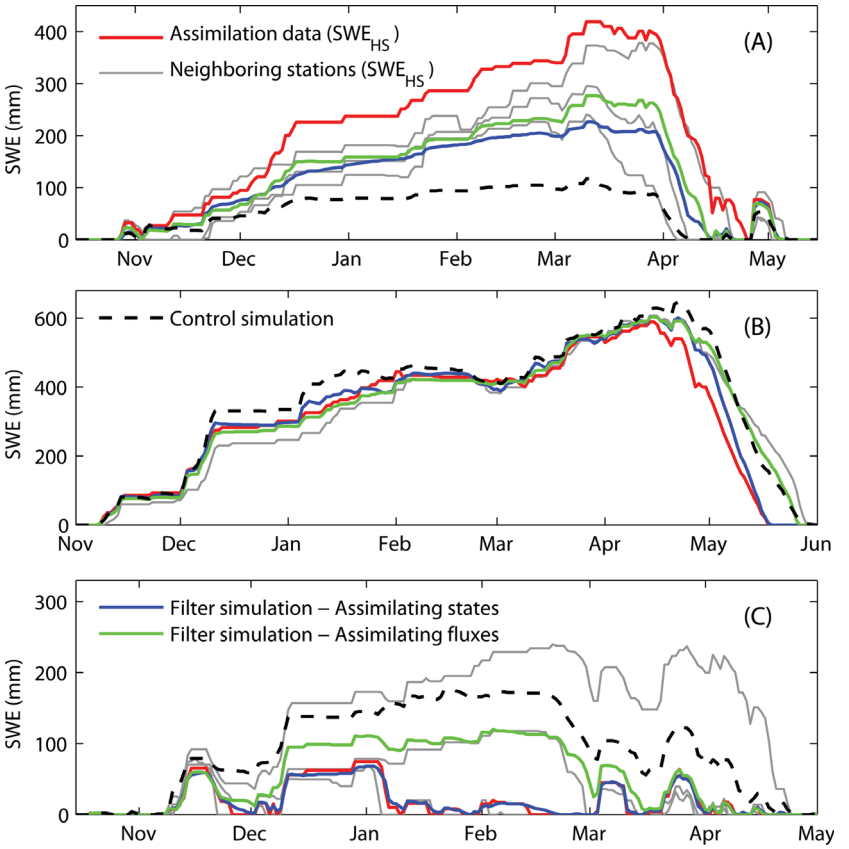

Figure 5. SWE time series at three different point locations with assimilation data available (subset of sites represented by crosses in Figure 1) including SWE_{HS} data from neighboring stations. The examples were chosen to demonstrate the behavior of both assimilation methods in scenarios where SWE is underestimated or overestimated.

precipitation event, the snowfall amounts are underestimated particularly along the transition from the lowland to the mountainous regions in the north (see the large difference in color between the station estimates represented by filled circles and the gridded estimates given in the background). The difference between the two snowfall estimates is also large in some inner alpine valleys. For this particular precipitation event, the discrepancies between the two estimates seem partly to arise from misclassification of precipitation type. Thus, the daily air temperatures may not have been representative for the duration of the precipitation event, a commonly occurring problem with snowfall estimates based on solely total precipitation and air temperature [*Feiccabrino et al.*, 2012]. The statistical interpolation scheme (see section 3.4.2) improves the simulated snowfall field compared to the control simulations (Figure 6, right). In particular, north of the alpine regions, the updated snowfall field matches the point estimates better than the control simulation (see the small color difference between the station values and the gridded estimates). The precipitation amounts in the eastern valleys also seem more realistic. Thus, for some precipitation events, the statistical interpolation scheme seems to remove large errors in simulated snowfall amounts.

4.3. Melt Rate Estimates

Temperature-index models typically reproduce melt rates over longer periods reliably (several days or longer) but sometimes fail for shorter time intervals [*Rango and Martinec*, 1995]. For some days, our simulation results using the temperature-index approach seem to display this behavior (Figure 7, left). The example shows that the control simulation results differ from the melt rates inferred from the point SWE data. The stations denoted by filled circles show overall higher melt rates than the gridded simulation results displayed in the background. We combine the temperature-index model simulations with point melt rates estimates using the ensemble Kalman filter (see section 3.4.2). The filter propagates information from the

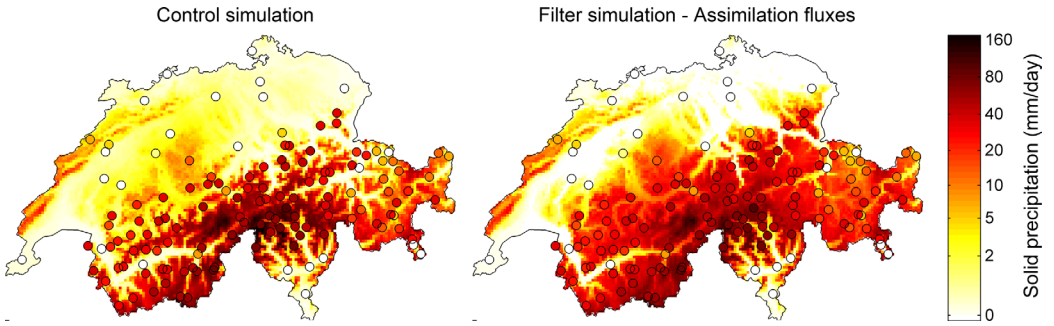

Figure 6. (left) Snowfall fields (8 December 2006) estimated from daily total precipitation and average air temperature, which were updated using (right) statistical interpolation. The filled circles show the snowfall amounts computed from snow water equivalent data compared to the gridded estimates plotted in the background.

station points to locations without any snow observations, and the updated gridded melt rates apparently follows the melt rate estimates closer than the control simulations (Figure 7, right).

4.4. Snow Water Equivalents

Figure 8 shows predicted against observed snow water equivalents for the four different experiments. The statistical metrics presented in the graphs were computed for each of the 45 stations separetely and afterward averaged over all observation sites. The figure additionally includes the range for the different statistical measures observed across the locations. The results show that the filter simulations appear to reproduce the observations with lower scatter than the control simulation. The mean-bias-errors deviated from zero for all methods, but none of those differences were statistically significant at $\alpha = 0.05$. The mean absolute error was lower for the two filter simulations (59.5 and 56.7 mm) than the control simulation (68.0 mm). However, the difference between the filter and control simulations was only statistically significant ($\alpha = 0.05$) for the flux assimilation method. The control simulation and interpolation methods showed similar results, whereas the latter display a slightly lower scatter for high snow water equivalent values than the control simulation. All hypothesis tests presented above were based on a two-sided Student *t* test with 44 degrees of freedom. The distributions of the examined variables were checked for normality before testing and if necessary transformed to closer match the normal distribution.

In two additional experiments, we investigated the influence of only assimilating one of the fluxes, either snowfall or melt rates derived from our daily SWE estimates. For those two experiments, the largest improvement compared to the control simulation was achieved by assimilating the snowfall amounts using statistical interpolation (MBE = 3.7 mm ranging from −134.1 to 142.4 mm between the stations, MAE = 58.4 mm ranging from 16.4 to 142.4 mm). The reduction in mean absolute error between the two methods is statistically significant at $\alpha = 0.05$ applying the same test as above. The assimilation of melt rates alone with the EnKF did not improve the model results (MBE = 18.9 mm ranging from −111.2 to 266.5 mm, MAE = 67.7 mm ranging from 20.1 to 266.5 mm). The main reason for explaining this behavior is that the melt model requires accurate snow amounts prior to ablation before the removing of errors in simulated melt rates

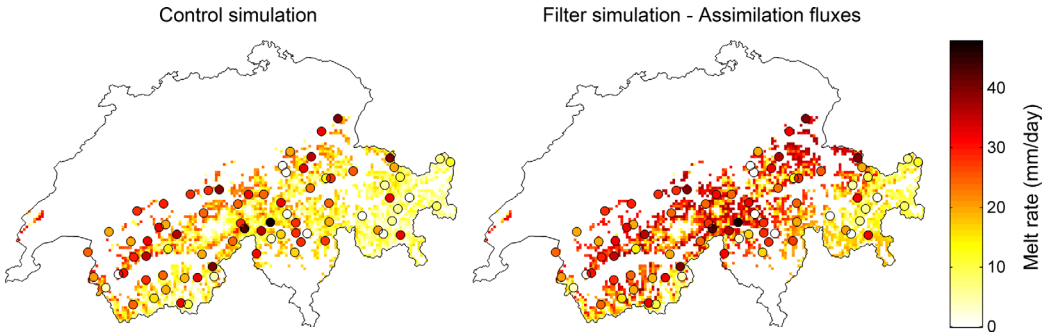

Figure 7. (left) Simulated gridded melt rates (5 May 2008) by the temperature-index model, which were updated using the (right) ensemble Kalman filter. The filled circles show the melt rates inferred from the daily snow water equivalent data.

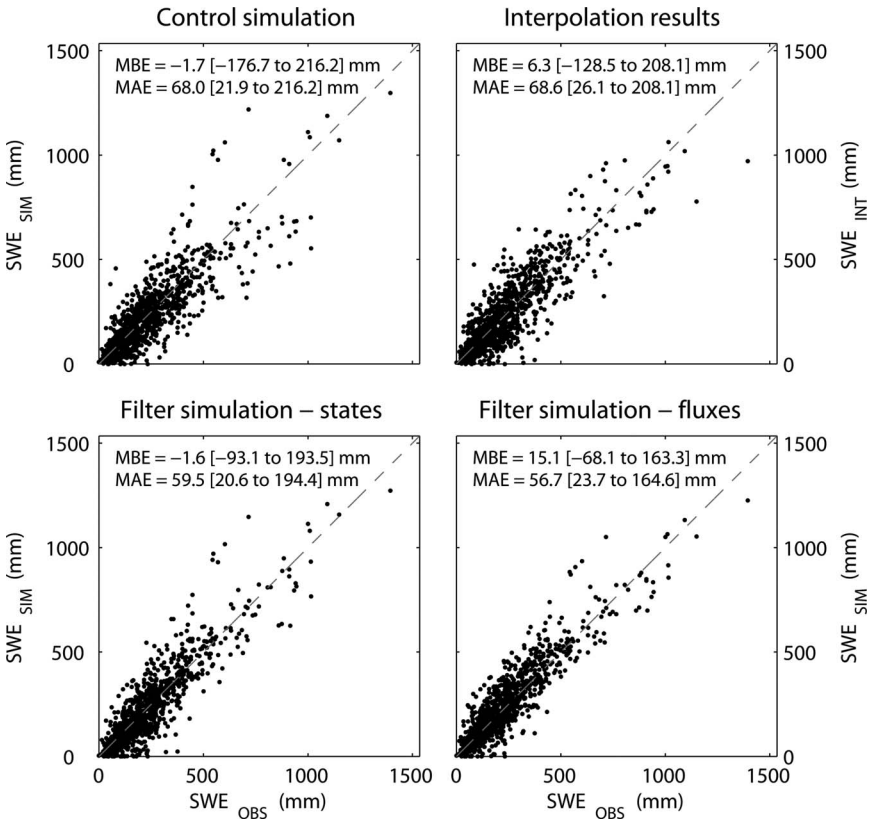

Figure 8. Scatterplots showing the control simulation, the interpolation method, and the two filter simulations against snow water equivalents observed at 45 stations providing 1033 samples together. The statistical measures (MBE: mean biased error and MAE: mean absolute error) were computed for each station separately and afterward averaged. The range in MBE and MAE across the sites is given within the brackets.

by assimilation improves the overall simulation quality. Thus, the combination of assimilating both quantities (snowfall and melt rates) may still be advantageous compared to only assimilating the snowfall amounts.

Figure 9 shows the performance (mean absolute error and squared correlation coefficient) observed at the 45 stations reporting snow water equivalent for the control simulation and two filter experiments in five categories. The state assimilation method reduces the number of stations with the largest errors (MAE $>$ 140 mm) compared to the control simulation (Figure 9, top), but does not show a large improvement for stations with lower errors (MAE $<$ 55 mm). The flux assimilation method, on the other hand, reduces the number of stations in both the medium and higher categories of mean absolute error (MAE $>$ 40 mm) resulting in more occurences in the lowest category (MAE $<$ 40 mm). Thus, the flux assimilation method seems to perform slightly better than the state assimilation method at stations where the errors in the control simulations already were modest (MAE $<$ 80 mm). All three simulations showed high correlation with the observations at most of the sites (Figure 9, bottom). The control simulation and state assimilation method showed similar correlation with the observations, whereas the flux assimilation appears to improve the linear association with the observations compared to the two other simulations. Thus, the later method may better capture the temporal dynamics of snow water equivalent than the remaining methods.

In the vicinity of stations, the four methods show similar SWE estimates (compare filled circles/squares representing station values with the gridded results shown in the background in Figure 10). Visually the difference is small between the control and the two filter simulation results. Between the temperature-index simulations and the benchmark method, the largest differences appear in some high elevated regions which largely lack snow observation sites. In such regions, the interpolation approach shows higher snow amounts than the three remaining results (compare, for example, the south-western regions between the plots in Figure 10). Those large snow amounts on high elevations results from the power function used in the interpolation for describing the vertical trend in SWE. Beyond altitudes higher than the stations ranges, this vertical trend may overestimate snow amounts.

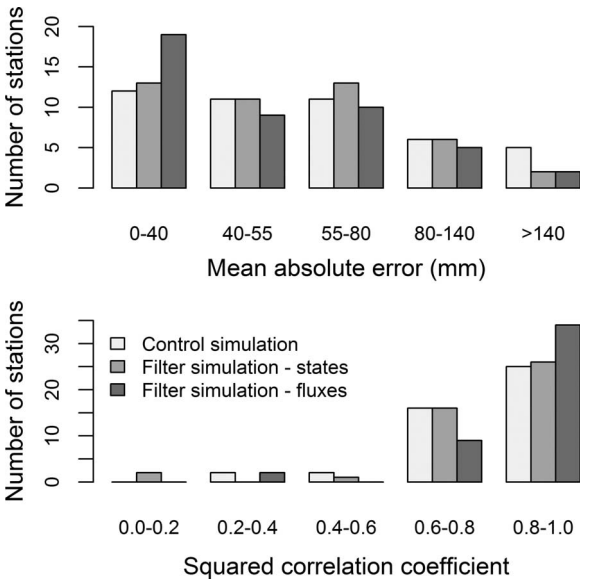

Figure 9. Histograms showing the number of stations within distinct categories of (top) mean absolute error and (bottom) squared correlation coefficient. The categories for MAE were defined by the 25th, 50th, 75th, and 90th percentiles of the control simulation results.

The simulation results when assimilating fluxes largely reproduce the spatial variations in SWE_{OBS} and SWE_{HS} around peak accumulation (compare filled circles/squares representing station values with the gridded results shown in the background in Figure 11, left). Some station values, however, differ from the simulated snow water equivalents fields. Such differences can arise because several stations are located several hundred vertical meters above or below the altitude of the digital elevation model used for the gridded simulations. Due to large altitude differences, a station recording does not need to display the same SWE as the underlying grid cell. In addition, stations can also be influenced by local processes, such as wind drift, and may not be representative for larger areas. The assimilation of fluxes should, however, to some extent dampen the influence of single inaccurate station readings since they are only used once for updating the model.

The differences between the filter and control simulations show systematic patterns between the years (Figure 11, right). In the lowland regions, the control simulation seems to overestimate the snow amounts. This behavior can partly be caused by the rather smooth curve describing the precipitation phase as a function

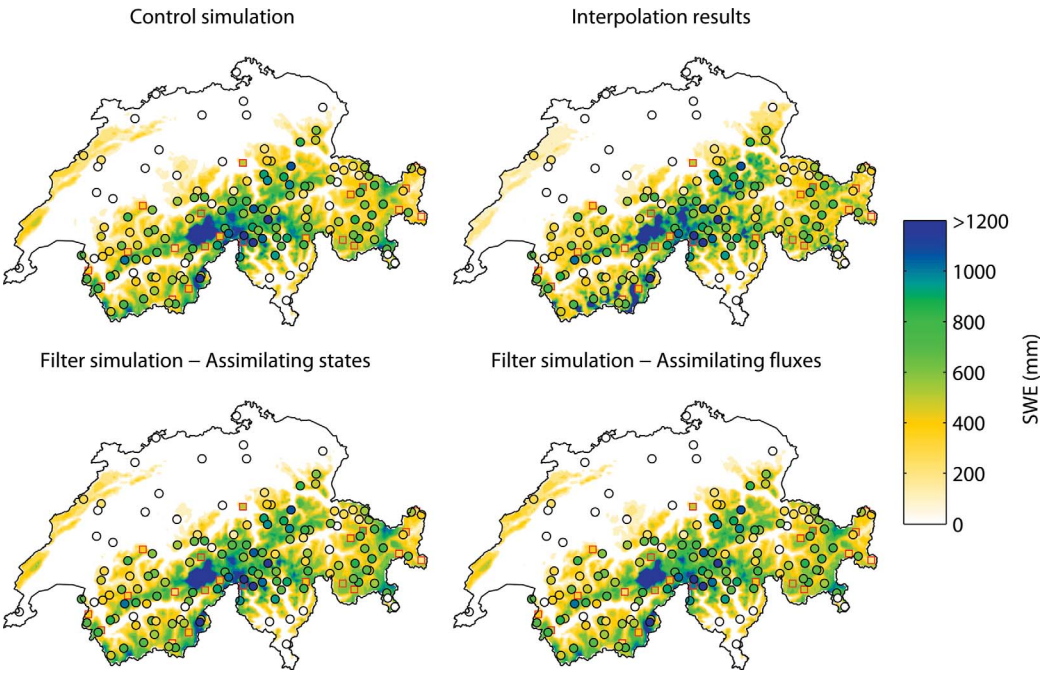

Figure 10. Comparison of snow water equivalent fields given by the four different methods around peak accumulation (15 March 2009). The squares with red edges indicate observed snow water equivalents and the circles with black edges display snow water equivalents estimated from snow depth observations (see section 3.1). The maps show a subset of all available stations for clarity.

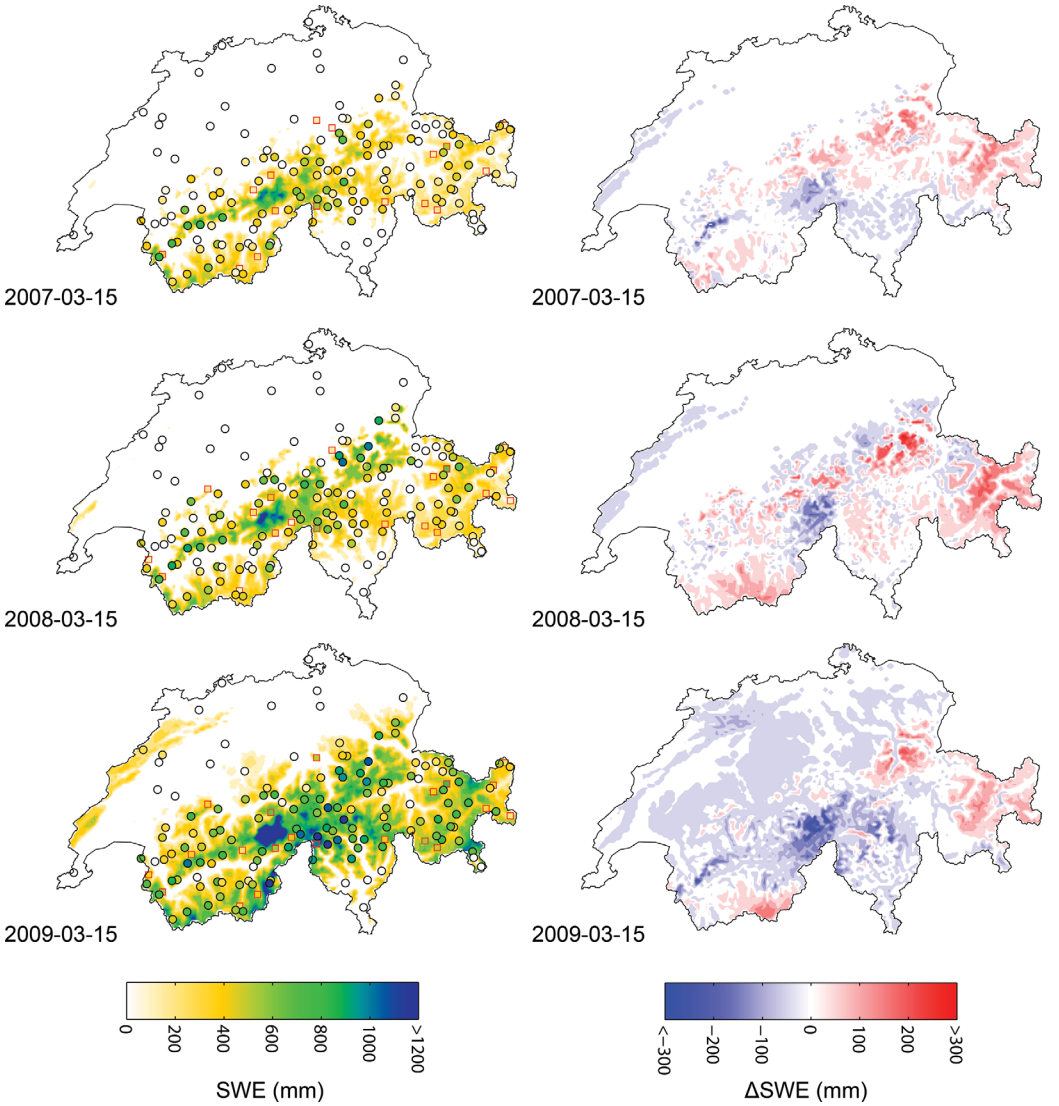

Figure 11. (left) The filter simulations in which we assimilate fluxes largely reproduce SWE_{OBS} (squares with red edges) and SWE_{HS} (circles with black edges) for the three study years. Large altitude differences between stations and the gridded model can cause large differences in snow water equivalent. The maps show a subset of all available stations for clarity. (right) The difference between filter and control simulations display some reoccurring patterns between the years, indicating systematic errors in the input data.

of air temperature. At low elevations, this simple precipitation model predicts too many snowfall events, and consequently overestimates snowfall. On higher elevations, the control simulations both underestimate and overestimate the snow amounts. In some areas, the precipitation correction factor accounting for undercatch is probably too low resulting in unrealistically low snow amounts. In other areas, the input may be biased in the opposite direction due to inaccurate altitudinal precipitation gradients. Thus, the statistical interpolation scheme does remove some biases in addition to random errors in the snowfall fields prior to assimilation of the melt rates. Strictly, the filter algorithm assumes background fields without systematic errors. However, both the background and the individual stations have systematic errors which may vary between seasons. Disentangling these biases is very difficult, and we therefore, at this stage, must accept that the statistical interpolation removes errors that may also feature a systematic component.

4.5. Snow-Covered Fraction

Overall, the results show that the simulations reliably reproduce the development of country-wide fractional snow-covered area throughout the study period (Figure 12). The simulations capture both the higher snow-covered fractions observed throughout the winter 2008/2009 with large snow amounts as well as the lesser

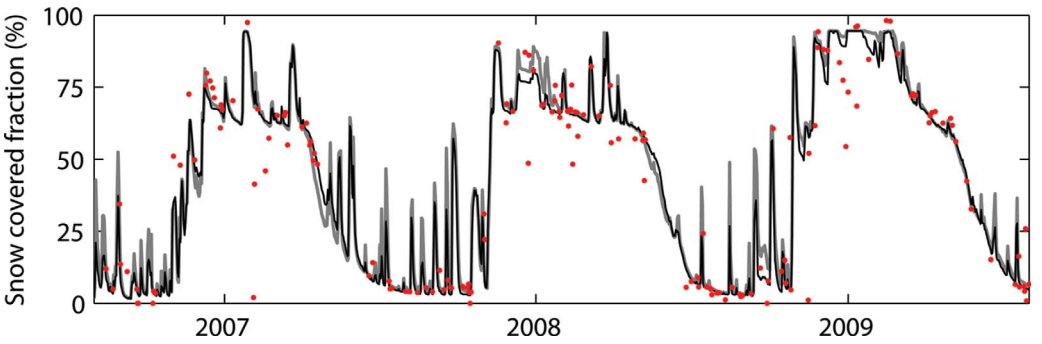

Figure 12. Observed (red dots) and simulated (gray line for the control simulation and black line for the flux assimilation method) fractional snow-covered area for the study region. The state assimilation method provides similar results as the other methods and is not shown for clarity. Satellite images showing more than 20% cloud coverage over the study area were removed from the analysis.

snow extents seen during the winter 2006/2007 with low snow amounts. During some short periods, for example, in the end of 2008, the model fails to capture the observations. For this particular event, the simulations seem unable to depict a melting episode reflected as a decline in observed fractional snow-covered area. In some other cases, discrepancies between the simulations and observation arose most likely due to large uncertainties in the observations from the satellite images.

The modeled fractional snow-covered area does not differ much between the control and flux assimilation experiment (Figure 12) even though the snow water equivalents differ largely between the two simulations in some regions (Figure 11, right). Overall, the three methods reproduce the observations with similar root-mean-squared errors varying between 11 and 12%. The largest differences in simulated snow-covered fraction occur during some snowfalls events, for which the filter simulations often show lower spikes than the control simulation. In many other situations, the two methods produce very similar results; a behavior which indicates that snow-covered area is largely insensitive to variations in snow water equivalent. Indeed, *Andreadis and Lettenmaier* [2006] showed that assimilating snow extent observations resulted in a modest improvement of SWE compared to a control simulation for regions with low snow amounts, whereas such improvements were missing in higher situated areas with more snow. At the same time, in higher situated regions with large snow accumulations, remote sensing products cannot provide reliable snow water equivalent observations [*De Lannoy et al*., 2012] and ground observations is in such regions therefore a valuable alternative.

5. Summary and Conclusions

In this study, we compare two methods for assimilating point SWE data into a distributed snow accumulation and melt model. In one experiment (called state assimilation), we use the ensemble Kalman filter to assimilate snow water equivalents which is a state variable in our model. In a second experiment (called flux assimilation), we compute snowfall and melt fluxes from the daily SWE data. We first update simulated snowfall rates using statistical interpolation and afterward update the model states using the ensemble Kalman filter for assimilating snowmelt rates. The two experiments give different results for several reasons, for example, (a) the flux assimilation method may use the finite ensemble size more efficiently than the state assimilation approach due to reduced forcing errors of the estimated snowfall rates and (b) the flexibility in defining error statistics is higher for the flux than the state assimilation method. For our study region, observations of snow cover development indicate that melt rates show less spatial variations than snowfall [*Egli and Jonas*, 2009; *Egli et al*., 2012]. We thus assume lower representativeness errors for the point estimates of melt rates than snowfall. This flexibility is not possible when assimilating snow water equivalents directly, and contributes to the differing results between the two methods.

Snow cover simulations usually show strong temporal autocorrelations, which also means that an error occurring in one time step can influence the simulation quality throughout the remaining winter. For example, a typical error with long persistence is mistakenly simulating a large snowfall episode as rainfall due to

inaccurate input data and/or model parameters. Thus, removing such errors in snow simulations is important for operational purposes relying on accurate initial conditions prior to prediction. We find that both data assimilation experiments reproduce observed snow water equivalents with lower errors than a control simulation. Assimilating fluxes (snowfall and melt rate estimates) yields slightly better results than when assimilating states (SWE estimates). Indeed, the error reduction is only statistically significant for the flux assimilation method but not for the state assimilation experiment. Since assimilation data were excluded in the neighborhood of the validation points, the results indicate that at least the flux assimilation method, which includes spatial error correlations, improves the results at unobserved locations. The control and filter simulations only show small differences in modeled fractional snow-covered area. However, this variable is only sensitive to changes in SWE in the case of a thin snow cover. Overall, both the control and filter simulation reliably reproduced the observed snow cover extent.

Our results illustrate how point SWE data can help in improving distributed SWE estimates using data assimilation if applied appropriately. For verifying the general applicability of the data assimilation methods presented in this study, the approaches should be adapted and tested for the available data and conditions in other regions. In particular, more effort should be invested in obtaining large-scale observations of snow water resources at repeated occasions by, for example, airborne laser-scanning measurements. Such observations would also be required for defining improved error estimates, needed for replacing the rough approximations used in this study.

Acknowledgments
The recommendations given by three reviewers improved the manuscript greatly. We also thank our colleagues L. Egli, C. Frei, J. W. Kirchner, C. Groot Zwaaftink, N. Griessinger, N. Helbig, and many more, who contributed with data processing, feedback, and good ideas. This study was partly funded by the Federal Office of the Environment FOEN.

References

Andreadis, K. M., and D. P. Lettenmaier (2006), Assimilating remotely sensed snow observations into a macroscale hydrology model, *Adv. Water Resour.*, *29*(6), 872–886.

Barnett, T. P., J. C. Adam, and D. P. Lettenmaier (2005), Potential impacts of a warming climate on water availability in snow-dominated regions, *Nature*, *438*(7066), 303–309.

Brown, R. D., B. Brasnett, and D. Robinson (2003), Gridded North American monthly snow depth and snow water equivalent for GCM evaluation, *Atmos. Ocean*, *41*(1), 1–14.

Clark, M. P., D. E. Rupp, R. A. Woods, X. Zheng, R. P. Ibbitt, A. G. Slater, J. Schmidt, and M. J. Uddstrom (2008), Hydrological data assimilation with the ensemble Kalman filter: Use of streamflow observations to update states in a distributed hydrological model, *Adv. Water Resour.*, *31*(10), 1309–1324.

Clark, M. P., J. Hendrikx, A. G. Slater, D. Kavetski, B. Anderson, N. J. Cullen, T. Kerr, E. O. Hreinsson, and R. A. Woods (2011), Representing spatial variability of snow water equivalent in hydrologic and land-surface models: A review, *Water Resour. Res.*, *47*, W07539, doi:10.1029/2011WR010745.

De Lannoy, G. J. M., R. H. Reichle, K. R. Arsenault, P. R. Houser, S. Kumar, N. E. C. Verhoest, and V. R. N. Pauwels (2012), Multiscale assimilation of advanced microwave scanning radiometer-EOS snow water equivalent and moderate resolution imaging spectroradiometer snow cover fraction observations in northern Colorado, *Water Resour. Res.*, *48*, W01522, doi:10.1029/2011WR010588.

de Rosnay, P., M. Drusch, D. Vasiljevic, G. Balsamo, C. Albergel, and L. Isaksen (2012), A simplified extended Kalman filter for the global operational soil moisture analysis at ECMWF, *Q. J. R. Meteorol. Soc.*, *139*(674), 1199–1213.

Egli, L., and T. Jonas (2009), Hysteretic dynamics of seasonal snow depth distribution in the Swiss Alps, *Geophys. Res. Lett.*, *36*, L02501, doi:10.1029/2008GL035545.

Egli, L., T. Jonas, T. Gruenewald, M. Schirmer, and P. Burlando (2012), Dynamics of snow ablation in a small Alpine catchment observed by repeated terrestrial laser scans, *Hydrol. Processes*, *26*(10), 1574–1585.

Essery, R., and J. Pomeroy (2004), Implications of spatial distributions of snow mass and melt rate for snow-cover depletion: Theoretical considerations, in *Annals of Glaciology*, vol. 38, edited by P. M. B. Fohn, pp. 261–265, International Symposium on Snow and Avalanches, 2-6 June, Davos, Switzerland.

Essery, R., S. Morin, Y. Lejeune, and C. B. Menard (2013), A comparison of 1701 snow models using observations from an alpine site, *Adv. Water Resour.*, *55*, 131–148.

Evensen, G. (2009), The ensemble Kalman filter for combined state and parameter estimation: Monte Carlo techniques for data assimilation in large systems, *IEEE Control Syst. Mag.*, *29*(3), 83–104.

Feiccabrino, J., A. Lundberg, and D. Gustafsson (2012), Improving surface-based precipitation phase determination through air mass boundary identification, *Hydrol. Res.*, *43*(3), 179–191.

Fletcher, S. J., G. E. Liston, C. A. Hiemstra, and S. D. Miller (2012), Assimilating MODIS and AMSR-E snow observations in a snow evolution model, *J. Hydrometeorol.*, *13*(5), 1475–1492.

Foppa, N., A. Stoffel, and R. Meister (2007), Synergy of in situ and space borne observation for snow depth mapping in the Swiss Alps, *Int. J. Appl. Earth Obs. Geoinf.*, *9*(3), 294–310.

Frei, C. (2013), Interpolation of temperature in a mountainous region using nonlinear profiles and non-Euclidean distances, *Int. J. Climatol.*, *34*, 1585–1605, doi:10.1002/joc.3786.

Frei, C., and C. Schar (1998), A precipitation climatology of the Alps from high-resolution rain-gauge observations, *Int. J. Climatol.*, *18*(8), 873–900.

Frei, C., R. Scholl, S. Fukutome, J. Schmidli, and P. L. Vidale (2006), Future change of precipitation extremes in Europe: Intercomparison of scenarios from regional climate models, *J. Geophys. Res.*, *111*, D06105, doi:10.1029/2005JD005965.

Harshburger, B. J., K. S. Humes, V. P. Walden, T. R. Blandford, B. C. Moore, and R. J. Dezzani (2010), Spatial interpolation of snow water equivalency using surface observations and remotely sensed images of snow-covered area, *Hydrol. Processes*, *24*(10), 1285–1295.

Huesler, F., T. Jonas, S. Wunderle, and S. Albrecht (2012), Validation of a modified snow cover retrieval algorithm from historical 1-km AVHRR data over the European Alps, *Remote Sens. Environ.*, *121*, 497–515.

Isotta, F. A., et al. (2013), The climate of daily precipitation in the Alps: Development and analysis of a high-resolution grid dataset from pan-Alpine rain-gauge data, *Int. J. Climatol.*, *34*, 1657–1675, doi:10.1002/joc.3794.
Jonas, T., C. Marty, and J. Magnusson (2009), Estimating the snow water equivalent from snow depth measurements in the Swiss Alps, *J. Hydrol.*, *378*(1–2), 161–167.
Kavetski, D., and G. Kuczera (2007), Model smoothing strategies to remove microscale discontinuities and spurious secondary optima in objective functions in hydrological calibration, *Water Resour. Res.*, *43*, W03411, doi:10.1029/2006WR005195.
Khlopenkov, K. V., and A. P. Trishchenko (2007), SPARC: New cloud, snow, and cloud shadow detection scheme for historical 1-km AVHHR data over Canada, *J. Atmos. Oceanic Technol.*, *24*(3), 322–343.
Kokkonen, T., H. Koivusalo, A. J. Jakeman, and J. Norton (2006), Construction of a degree-day snow model in the light of the 10 iterative steps in model development, in *Proceedings of the iEMSs Third Biennial Meeting: Summit on Environmental Modelling and Software* [CD-ROM], edited by A. Voinov, A. J. Jakeman, and A. E. Rizzoli, 12 pp., Int. Environ. Modell. and Software Soc., Burlington, Vermont.
Leisenring, M., and H. Moradkhani (2011), Snow water equivalent prediction using Bayesian data assimilation methods, *Stochastic Environ. Res. Risk Assess.*, *25*(2), 253–270.
Li, L., and S. P. Simonovic (2002), System dynamics model for predicting floods from snowmelt in North American prairie watersheds, *Hydrol. Processes*, *16*(13), 2645–2666.
Liston, G. E., and C. A. Hiemstra (2008), A simple data assimilation system for complex snow distributions (SnowAssim), *J. Hydrometeorol.*, *9*(5), 989–1004.
Liston, G. E., R. A. Pielke, and E. M. Greene (1999), Improving first-order snow-related deficiencies in a regional climate model, *J. Geophys. Res.*, *104*(D16), 19,559–19,567.
Liu, Y., et al. (2012), Advancing data assimilation in operational hydrologic forecasting: Progresses, challenges, and emerging opportunities, *Hydrol. Earth Syst. Sci.*, *16*(10), 3863–3887.
Liu, Y., C. D. Peters-Lidard, S. Kumar, J. L. Foster, M. Shaw, Y. Tian, and G. M. Fall (2013), Assimilating satellite-based snow depth and snow cover products for improving snow predictions in Alaska, *Adv. Water Resour.*, *54*, 208–227.
Lopez-Moreno, J. I., and D. Nogues-Bravo (2006), Interpolating local snow depth data: An evaluation of methods, *Hydrol. Processes*, *20*(10), 2217–2232.
Marks, D., and A. Winstral (2001), Comparison of snow deposition, the snow cover energy balance, and snowmelt at two sites in a semiarid mountain basin, *J. Hydrometeorol.*, *2*(3), 213–227.
Martinec, J., and A. Rango (1991), Indirect evaluation of snow reserves in mountain basins, edited by H. Bergmann, H. Lang, W. Frey, D. Issler, and B. Salm, in Proceedings: Snow, Hydrology and Forest in High Alpine Areas, *205*, 111–120, IAHS Publication, Vienna.
Ohmura, A. (2001), Physical basis for the temperature-based melt-index method, *J. Appl. Meteorol.*, *40*(4), 753–761.
Oke, P. R., P. Sakov, and S. P. Corney (2007), Impacts of localisation in the EnKF and EnOI: Experiments with a small model, *Ocean Dyn.*, *57*(1), 32–45.
Pulliainen, J. (2006), Mapping of snow water equivalent and snow depth in boreal and sub-arctic zones by assimilating space-borne microwave radiometer data and ground-based observations, *Remote Sens. Environ.*, *101*(2), 257–269.
Rango, A., and J. Martinec (1995), Revisiting the degree-day method for snowmelt computations, *Water Resour. Bull.*, *31*(4), 657–669.
Reichle, R. H., and R. D. Koster (2003), Assessing the impact of horizontal error correlations in background fields on soil moisture estimation, *J. Hydrometeorol.*, *4*(6), 1229–1242.
Schaefli, B., B. Hingray, and A. Musy (2007), Climate change and hydropower production in the Swiss Alps: Quantification of potential impacts and related modelling uncertainties, *Hydrol. Earth Syst. Sci.*, *11*(3), 1191–1205.
Schwarb, M., C. Daly, C. Frei, and C. Schär (2001), Mean annual and seasonal precipitation in the European Alps 1971–1990, in *Hydrological Atlas of Switzerland*, edited, Univ. of Bern, Bern, Switzerland.
Shepard, D. S. (1984), Computer mapping: The SYMAP interpolation algorithm, *Spatial Stat. Models*, *40*, 133–145.
Slater, A. G., and M. P. Clark (2006), Snow data assimilation via an ensemble Kalman filter, *J. Hydrometeorol.*, *7*(3), 478–493.
Stewart, I. T., D. R. Cayan, and M. D. Dettinger (2004), Changes in snowmelt runoff timing in western North America under a 'business as usual' climate change scenario, *Clim. Change*, *62*(1–3), 217–232.
Tobin, C., B. Schaefli, L. Nicotina, S. Simoni, G. Barrenetxea, R. Smith, M. Parlange, and A. Rinaldo (2013), Improving the degree-day method for sub-daily melt simulations with physically-based diurnal variations, *Adv. Water Resour.*, *55*, 149–164.
Uboldi, F., C. Lussana, and M. Salvati (2008), Three-dimensional spatial interpolation of surface meteorological observations from high-resolution local networks, *Meteorol. Appl.*, *15*(3), 331–345.
Weerts, A. H., and G. Y. H. El Serafy (2006), Particle filtering and ensemble Kalman filtering for state updating with hydrological conceptual rainfall-runoff models, *Water Resour. Res.*, *42*, W09403, doi:10.1029/2005WR004093.